Materials Research. 2025; 28: e20250205
DOI: https://doi.org/10.1590/1980-5373-MR-2025-0205

Understanding the Influence of Aging Time on the Eutectic Growth of Sn-xBi Solder Alloys

S. L. A. Dantas[a], Bruno Sobral[a], A. Garcia[b], J. E. Spinelli[c], B. L. Silva[a]*

[a]*Universidade Federal do Rio Grande do Norte (UFRN), Departamento de Engenharia de Materiais, 59078-970, Natal, RN, Brasil.*
[b]*Universidade de Campinas (UNICAMP), Departamento de Engenharia de Manufatura e Materiais, 13083-860, Campinas, SP, Brasil.*
[c]*Universidade Federal de São Carlos (UFSCar), Departamento de Engenharia de Materiais, 13565-905, São Carlos, SP, Brasil.*

Received: January 29, 2025; Revised: May 15, 2025; Accepted: June 08, 2025

In order to support new packaging technologies driven by new demands for rapid data communication in 5G and IoT (Internet of Things), as well as prevent issues related to thermal expansion and deformation. Studies aimed at understanding the effect of temperature and time during service life of soldered parts are rare, especially for the Sn/Bi eutectic arrangement. Therefore, this study aims to understand the influence of the aging time (30, 60 and 90 days) at 100 °C on the local eutectic coarsening of Sn-xBi alloys (x=34, 52 and 58 wt.% Bi). Directionally solidified samples, solidified at cooling rates compatible with soldering, were examined using SEM with the aid of Energy-dispersive X-ray spectroscopy analysis, and Vickers hardness tests to assess both untreated and treated eutectic microstructures. The sample having lower Bi content showed higher coarsening sensitivity over time due to increased Bi flow from the β-Sn phase to the eutectic Bi.

Keywords*: Solidification, Sn-Bi alloys, eutectic coarsening, aging treatment.*

1. Introduction

The issue of microstructural stability in solder alloys has been extensively investigated by various researchers[1-4]. Anderson et al.[1] demonstrated that the addition of Co to Sn-Ag-Cu alloys not only acted as a solidification catalyst, promoting enhanced microstructural refinement, but also contributed to improved microstructural stability and mechanical strength retention by modifying the coarsening behavior of solder joints during high-temperature aging. Moreover, considerable research has been dedicated to examining the effects of elemental doping on the microstructural stability of Sn-Cu alloys at elevated temperatures[2-4].

Despite existing studies on Bi precipitation in Sn-rich solder alloys aged at room temperature[5-9], data on the coarsening behavior of Bi at higher temperatures remain scarce. Previous investigations have focused on the coarsening of Bi particles in SAC-Bi/Cu, Sn-Ag-Bi/Cu, and Sn-Bi/Cu solder joints subjected to room-temperature aging[5-9]. Belyakov et al.[6] observed the growth of Bi plates as a function of aging time, while Wu et al.[7] conducted an in-depth study to elucidate the microstructural evolution, particularly the Bi coarsening process, in SAC-3Bi solder alloys during room-temperature aging.

Soldered joints play a critical role in the electronics industry by ensuring both mechanical strength and electrical conductivity, thus ensuring the reliability of electronic components[10-12]. The properties/features of solder alloys and interfacial layers have a significant impact on solder joints and consequently affect the performance of electronic devices. Traditional solder alloys, primarily based on lead-tin alloys, are being reconsidered due to lead toxicity, leading to the exploration of more sustainable alternatives like hypoeutectic and eutectic Sn-Bi alloys[10,12-22].

The interconnects in electronic packages not only suffer thermal shocks caused by changes in ambient temperature, but also the elevated temperature induced by Joule heating. Therefore, the thermal stability and performance of solder interconnects have become one of the important indicators of their reliability. The aging of welded joints is a thermal process that occurs when the material is exposed to temperatures between 50 and 100 °C for hours and/or days, causing significant microstructural and property changes[6,8]. Several types of damages are possible in joints, including joint movement and shocks, fatigue fail, corrosion action, and coarsening of either the alloy microstructure or the interfacial layer[23].

Besides the obvious interest in microstructure stability in the soldering sector, more recently, bismuth-containing alloys have been envisaged for new applications such as plugs for oil well capping and closure operations, since this metal expands when it solidifies[24], and has the potential to outperform cement. In this scenario, Sn-Bi alloys are potential alternatives for such applications. Operating temperatures can reach up to 100-130 °C, and the aging characteristics of the alloys are essential to enable their use as a sealing material.

*e-mail: bismarck.silva@ufrn.br
Associate Editor: Hugo Sandim.
Editor-in-Chief: Luiz Antonio Pessan.

Despite the importance of microstructure coarsening in understanding the behavior of solder joints, most studies primarily focus on macroscopic behaviors, leaving a notable research gap, especially concerning the coarsening of eutectic Sn-Bi alloys subjected to thermal cycling[25-27].

Compared to Sn-Ag-Cu and Sn-Ag based solders, Sn-Bi solders undergo more pronounced microstructural changes when subjected to thermal loads[28,29]. The evolution of microstructure in Sn-Bi joints can occur even under room temperature storage conditions[30], and the coarsening of phases may result in decreased mechanical strength for Sn-Bi solder joints[31]. Due to their low melting points, Sn-Bi alloys exhibit a high homologous temperature. For example, the homologous temperature of the Sn-Bi eutectic solder (Sn–58wt.% Bi) at 100 °C is 0.9, making microstructural coarsening more readily observable.

The present investigation aims to fill the mentioned gap by exploring how long-time aging treatment affects the scale of the eutectic microstructure of Sn-(x)Bi alloys, considering starting eutectic structures produced at high solidification cooling rates to provide insights into their thermal stability and mechanical strength.

2. Materials and Methods

The Sn-34 wt.% Bi, Sn-52 wt.% Bi, and Sn-58 wt.% Bi alloys were produced using commercially pure tin (Sn-99.88%) and bismuth (Bi-99.99%). These metals were melted following adequate quantities in an Inductotherm VIP model power-trak 50-30 R induction furnace to produce the binary alloys. A vertical directional solidification process was employed, utilizing a vertical furnace with top-to-bottom directional cooling. A water-cooled upward unidirectional solidification device with a 3 mm thick carbon steel plate (SAE 1020) at the bottom allowed heat extraction, while a two-part stainless-steel mold with inner insulation minimized radial heat loss. J-type thermocouples coated with stainless steel tubes were used to monitor temperature evolution during solidification of each alloy, connected to an Almemo thermal data logger (model 2890-8) for real-time temperature measurements and data storage[16,32,33].

The temperature × time data obtained were used to determine the solidification cooling rate at different points along the length of each produced casting. Samples of each alloy were collected from the position with the finest eutectic arrangement, in order to analyze how much this microstructure could be altered by thermal aging. The samples of each alloy were chosen at 5 mm from the metal/mold interface. After cross-cutting the castings, samples measuring approximately 1.0 cm^2 in area and 1.0 mm thick of each alloy were taken to carry out the aging process of heat treatment, as shown in Figure 1.

The choice of the position 5 mm close to the cooled base was due to these samples exhibit the highest cooling rates in each Sn-Bi alloy, and consequently, cooling rates closer to the values found in soldered joints in electronic microcomponents. Typical cooling rates during reflow procedures for solders in industrial practice remain in the range of 3.0–10.0 K/s[34,35].

But considering specifically the Sn-Bi alloys of the present study, the cooling rates varied between 0.1 and 12.0 °C/s, as reported by Silva et al.[33]. The cooling rates were determined from the direct reading of the quotient of the temperatures immediately before and after the *liquidus* temperature (T_L) and the corresponding *liquidus* front passage times at each position of the castings, i.e., $\dot{T}_L = \Delta T/\Delta t$.

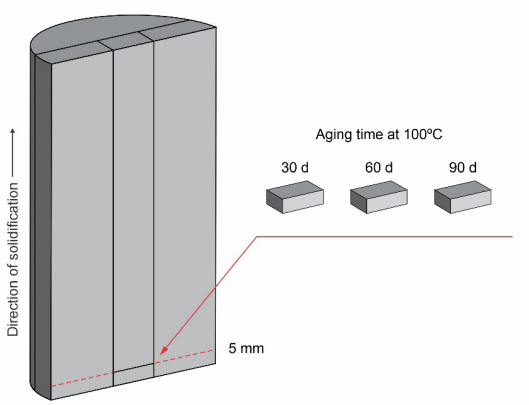

Figure 1. Scheme of the longitudinal section of the directionally solidified casting and the sample removal, including the thermal aging conditions (temperature and time).

Samples extracted at 5 mm from the cooled bottom of the three alloys castings underwent aging heat treatments in an oven (Rectangular model, Tramontina) at a fixed temperature of 100 °C for 30, 60, and 90 consecutive days. This temperature was chosen to induce a more accelerated aging of the alloys, which is an approximation of what actually occurs when using electronic equipment with soldering joints. 90-day time has been chosen based on 2 reasons: testing a longer comparative effect of aging time, in order to find a limit time that affects eutectic growth; 2. empirically simulating the lifetime of electronic components using Sn-Bi solder alloys. The value of 100 °C for the aging temperature was chosen based on literature values for tin-based alloys[36-40]. Metallographic procedures were then performed, including sanding, polishing, micro-etching (100 mL of distilled H_2O, 2.5 mL of HC*l* and 10 g of Fe$C*l*_3$ for 30 s), and scanning electron microscopy (SEM-EDS - Auriga 40 model) to analyze microstructural coarsening as a function of time and determine the eutectic spacing (λ). In order to obtain mean and average deviation λ values, 40 measurements were carried out for each microstructural configuration studied, applying the method proposed by McCartney and Hunt[41]. Hardness tests were performed on the transversal sections at different points of the eutectic microstructure using a test load of 100 gf and a count time of 10 s. Eight measurements have been performed per sample analyzed with a statistical treatment to obtain a mean value and standard deviation.

3. Results and Discussion

Figure 2 illustrates the eutectic microstructure characteristics of the Sn-Bi samples before and after aging for 90 days. Bi is the darker phase in the images in Figure 2, and although the eutectic complex structure

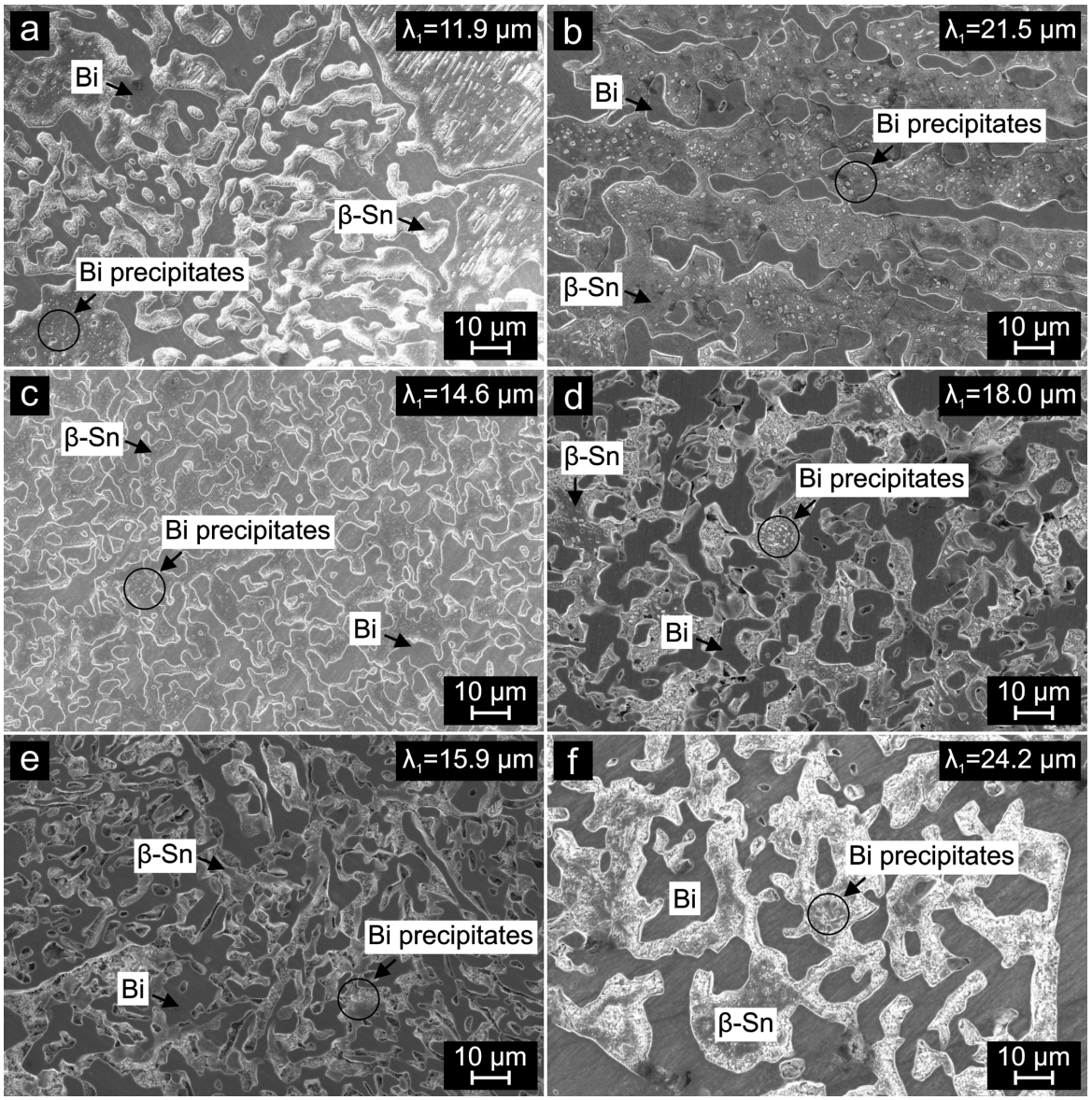

Figure 2. Micrographs of the eutectic microconstituent in untreated (a) Sn-34wt.% Bi, (c) Sn-52wt.% Bi, (e) and Sn-58wt.% Bi, and treated (b) Sn-34wt.% Bi, (d) Sn-52wt.% Bi, and (f) and Sn-58wt.% Bi alloys samples. The images in (b,d,f) correspond to the treated samples for 90 days at 100 °C.

is roughly maintained, some thickening happened with aging as translated by the λ values. Figure 2(a,c,e) shows samples originally solidified at high cooling rates, while Figure 2(b,d,f) subsequently aged samples. This growth is driven by diffusion, prompting the migration of atoms from the Bi eutectic phase to the Sn-rich phase.

Comparing the microstructures of all the alloys analyzed, it is noted that the Sn-34wt.%Bi alloy displays higher fractions of the Sn-rich primary phase, which was already expected as it is a hypoeutectic composition. The opposite occurs for the Sn-58wt.%Bi alloy, as it is the eutectic composition for the Sn-Bi system. It is also observed that the morphology of Bi particles dispersed in the Sn-rich phase tends to be more lamellar for longer aging heat treatment times. The same effect was reported by Nishikawa et al.[42] in the study of heat-treated Sn-45wt.%Bi, Sn-45wt.%Bi-2.6wt.%Zn, Sn-45wt.%Bi-2.6wt.%Zn-0.5wt.%In alloys with an aging time of 42 days. Considering the Sn-45 wt.% Bi alloy, the authors observed that after aging, both β-Sn and the Bi phase went from a refined to a coarse condition.

Given that Bi is the primary diffusion element in Sn–Bi solders[43], the growth in the Sn-rich phase is significantly less than in the Bi-rich phase. Consequently, the diffusion of Sn atoms may have minimal impact on the microstructure and properties during thermal aging. Heat treatment deals with the acceleration of the diffusion process, which is also a compromise between the employed temperature, time and the paths for diffusion characterizing the microstructure.

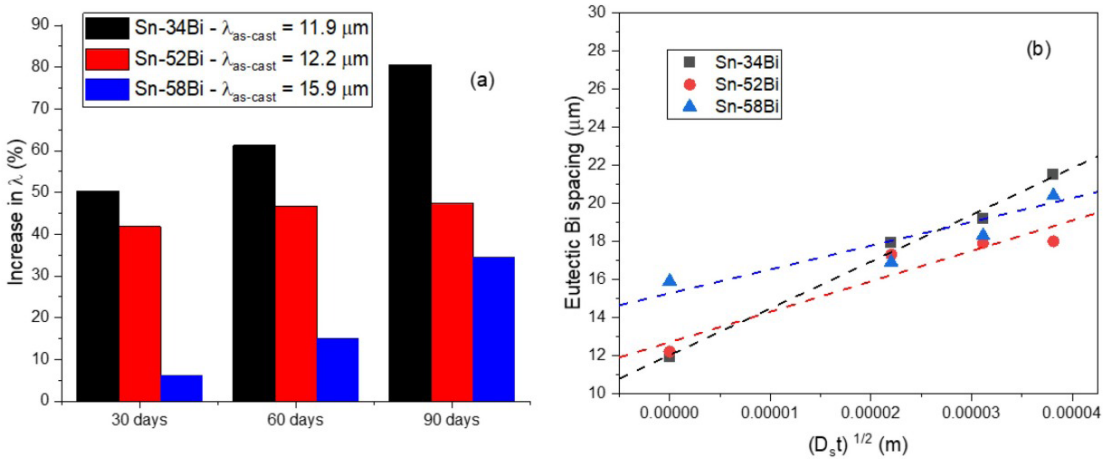

Figure 3. (a) Percentage evolution of λ as a function of aging period, and (b) λ as a function of $(D_s \times t)^{1/2}$ for the Sn-Bi alloy samples.

The diffusion process has a greater potential for growth in refined samples due to the higher number of phase boundaries, which serve as diffusion sites. This accounts for the substantial coarsening of λ observed in the refined initial dendritic microstructures, as can be seen in Figure 3a, especially in the case of the Sn-34 wt.% Bi alloy. After 90 days, the original λ of 11.9 μm increased by approximately 80.6%. This growth was governed by the diffusion process, which stimulates the migration of atoms from fine eutectic boundaries to neighboring ones, forming coarser structures.

Minho et al.[44] confirmed that heat treatment time directly influences the microstructure of intermetallic layers and the eutectic mixture in Sn-58wt.%Bi, Sn-57 wt.%Bi-1wt.%Ag, and Sn-57wt.%Bi-1wt.%Ni alloys. With increased heat treatment time, the Bi layers in the eutectic structure tended to become coarser, as also observed here. Aged eutectic structures exhibited a more heterogeneous and random distribution and morphology as compared to the untreated samples, as can be seen in Figure 2.

Coarsening is quite sensitive to the initial microstructure features and composition, as it can be seen in the evolution in Figure 3. The percentage increase in λ decreased as the Bi content increased. To understand the initial distribution of Bi before the heat treatment, five EDS point measurements for each alloy were performed on eutectic Sn lamellae in regions where Bi is in solution, as seen in Figures 4a-c. A much higher Bi content in the β-Sn phase was found in the Sn-34 wt.% Bi alloy, which induced a higher Bi flow in this alloy, promoting higher coarsening over time. Bi enter in solid solution and diffuse throughout Sn. At temperatures above the solvus, a homogeneous dispersion of Bi precipitates forms, as shown in Figure 2. Elevated temperatures will accelerate this process, as the solubility of Bi in Sn increases with temperature[45].

Considering that the diffusion length is proportional to the square root of the mobility lifetime $(D_S \times t)^{1/2}$, the λ results were plotted against this parameter as shown in Figure 3b. Here, D_s represents the solid diffusion coefficient (in m^2/s), which is approximately 1.87×10^{-16} m^2/s for Bi in the β-Sn phase for Sn-Bi alloys[46]. Equations were derived, yielding coefficients of determination (R^2) greater than 0.8, demonstrating strong agreement between the trends and the experimental data. The lines in Figure 3b refer to these equations.

The analysis of hardness with respect to the alloy Bi content and microstructure is important to assess their effect on the mechanical strength. Generally, phase coarsening reduced hardness, as seen in the comparison between as-cast and as-aged bars in Figure 4d. For alloys with a higher fraction of the Sn phase (i.e., Sn-34 and 52Bi), there was a notable decrease in hardness due to the thickening of Bi precipitates in the Sn-rich phase. In contrast, the Sn-58 wt.% Bi alloy showed a slight increase in hardness after aging due to the increased width of the eutectic Bi phase. It is worth noting that the Sn-58 wt.% Bi alloy has lower β-Sn phase fraction as compared to the other alloys examined. As such, the thickening of the Bi precipitates within the β-Sn phase has a negligible effect in this case.

The mean values of the Vickers indentation diagonals in the untreated and aged samples are 95.4 μm and 97.3 μm, respectively. The dispersion of the mean Vickers microhardness values is associated with the fraction of the Sn-rich phase, Bi content and thickening of the Bi-rich phase. The decrease in hardness after 90 days of aging time occurred for the Sn-34wt.%Bi and Sn-52wt.%Bi alloys due to the thickening of the Bi-rich phase. This behavior was more evident considering that these alloys exhibit higher fractions of the Bi-rich phase.

The limitation of SEM-EDS may arise from the electron beam interaction volume, which extends beneath the surface of the sample. This causes signal mixing from adjacent phases and subsurface regions, reducing spatial resolution and the accuracy of compositional analysis[47]. Despite this interaction and some possible variations in the measured wt. % values in Figure 4a, the trend of higher Bi content in the eutectic Sn lamellae for lower alloy content remains evident, as explained above.

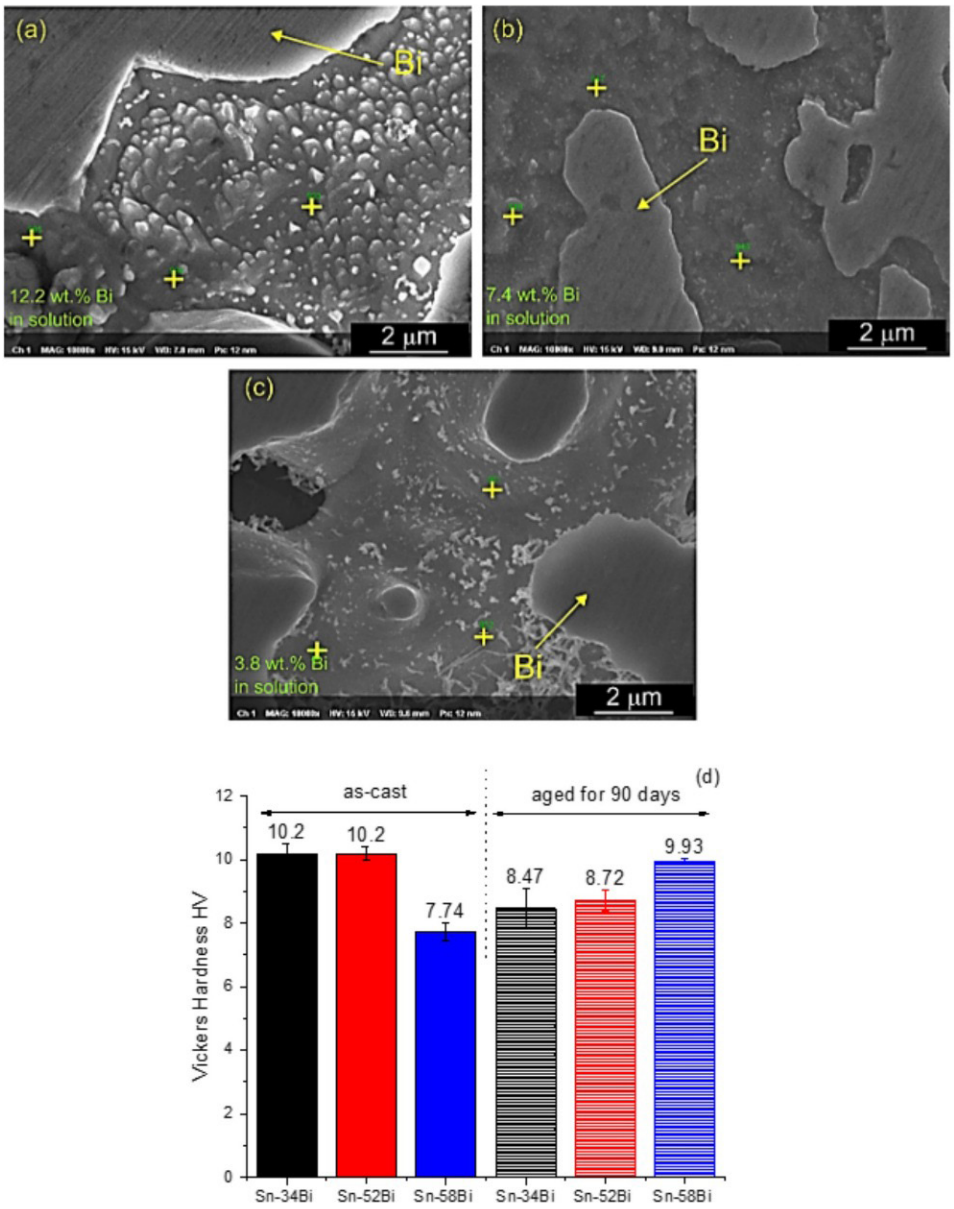

Figure 4. (a,b,c) SEM-EDS data measured of Bi in solution in the eutectic Sn phase considering untreated samples; and (d) hardness in both treated and untreated Sn-Bi samples.

4. Conclusions

- Comparing the microstructures of all the alloys analyzed, it is shown that the Sn-34wt.%Bi alloy displays higher fractions of the Sn-rich primary phase. The opposite occurs for the Sn-58wt.%Bi alloy, as it is the eutectic composition for the Sn-Bi system.
- Coarsening was shown to be quite sensitive to the initial microstructure features and Bi content of the alloy. The percentage increase in λ decreased as the alloy Bi content increased.
- For alloys with a higher fraction of the Sn phase (i.e., Sn-34Bi and Sn-52Bi), after aging for 90 days there was a decrease in hardness of about 17% and 14.5%, respectively, due to the thickening of Bi precipitates in the Sn-rich phase. In contrast, the Sn-58Bi alloy showed a 28.3% increase in hardness after aging due to the increased width of the eutectic Bi phase.

5. Acknowledgments

The authors acknowledge FAPESP (grant 2023/06107-3) and CNPq. This study was financed in part by the Coordenação de Aperfeiçoamento de Pessoal de Nível Superior - Brasil (CAPES) - Finance Code 001.

6. References

1. Anderson IE, Foley JC, Cook BA, Harringa J, Terpstra RL, Unal O. Alloying effects in near-eutectic Sn-Ag-Cu solder alloys for improved microstructural stability. J Electron Mater. 2001;30(9):1050-9. http://doi.org/10.1007/s11664-001-0129-5.
2. Ventura T, Cho Y, Kong C, Dahle AK. Formation of intermetallics in Sn-0.9Cu and Sn-0.7Cu-0.08Ni solders. J Electron Mater. 2011;40(6):1403-8. http://doi.org/10.1007/s11664-010-1496-6.
3. Yu C, Chen W, Duh J. Suppressing the growth of Cu-Sn intermetallic compounds in Ni/Sn-Ag-Cu/Cu-Zn solder joints during thermal aging. Intermetallics. 2012;26:11-7. http://doi.org/10.1016/j.intermet.2012.03.046.
4. Hassan KR, Wu J, Alam MS, Suhling JC, Lall P. Mechanical behavior and reliability of SAC+Bi lead-free solders with various levels of bismuth. In: 2021 IEEE 71st Electronic Components and Technology Conference (ECTC); 2021; San Diego, CA, USA. Proceedings. New York: IEEE; 2021. p. 937-45.
5. El-Daly AA, El-Taher AM, Gouda S. Novel Bi-containing Sn-1.5Ag-0.7Cu lead-free solder alloy with further enhanced thermal property and strength for mobile products. Mater Des. 2015;65:796-805. http://doi.org/10.1016/j.matdes.2014.10.006.
6. Belyakov SA, Xian J, Zeng G, Sweatman K, Nishimura T, Akaiwa T, et al. Precipitation and coarsening of bismuth plates in Sn-Ag-Cu-Bi and Sn-Cu-Ni-Bi solder joints. J Mater Sci Mater Electron. 2019;30(1):378-90. http://doi.org/10.1007/s10854-018-0302-8.
7. Wu JA, Luktuke A, Chawla N. Surface precipitation and growth of bismuth particles in Sn-Ag-Cu-Bi solder joints. J Electron Mater. 2023;52(2):801-9. http://doi.org/10.1007/s11664-022-10126-7.
8. Wang F, Luktuke A, Chawla N. Microstructural coarsening and mechanical properties of eutectic Sn-58Bi solder joint during aging. J Electron Mater. 2021;50(12):6607-14. http://doi.org/10.1007/s11664-021-09255-2.
9. Vianco PT, Rejent JA. Properties of ternary Sn-Ag-Bi solder alloys: part I - thermal properties and microstructural analysis. J Electron Mater. 1999;28(10):1127-37. http://doi.org/10.1007/s11664-999-0250-4.
10. Zhu W, Zhang W, Zhou W, Wu P. Improved microstructure and mechanical properties for SnBi solder alloy by addition of Cr powders. J Alloys Compd. 2019;789:805-13. http://doi.org/10.1016/j.jallcom.2019.03.027.
11. Yang L, Zhu L, Zhang Y, Zhou S, Wang G, Shen S, et al. Microstructure, IMCs layer and reliability of Sn-58Bi solder joint reinforced by Mo nanoparticles during thermal cycling. Mater Charact. 2019;148:280-91. http://doi.org/10.1016/j.matchar.2018.12.012.
12. Yen YW, Syu RS, Chen CM, Jao CC, Chen GD. Interfacial reactions of Sn–58Bi and Sn–0.7Cu lead-free solders with Alloy 42 substrate. Microelectron Reliab. 2014;54(1):233-8. http://doi.org/10.1016/j.microrel.2013.09.003.
13. Dhand V, Han G, Kim S, Rhee K. Effect of nano-phased bismuth–tin alloy surface coating on tribo-mechanical properties of basalt fiber reinforced composites. J Mater Res Technol. 2022;21:2238-46. http://doi.org/10.1016/j.jmrt.2022.10.006.
14. Frongia F, Pilloni M, Scano A, Ardu A, Cannas C, Musinu A, et al. Synthesis and melting behaviour of Bi, Sn and Sn–Bi nanostructured alloy. J Alloys Compd. 2015;623:7-14. http://doi.org/10.1016/j.jallcom.2014.08.122.
15. Shen YA, Zhou S, Li J, Tu KN, Nishikawa H. Thermomigration induced microstructure and property changes in Sn-58Bi solders. Mater Des. 2019;166:107619. http://doi.org/10.1016/j.matdes.2019.107619.
16. Paixão JL, Sousa RB, Sobral BS, Sousa RM, Luz JRD, Spinelli JE, et al. Zn additions modifying microstructure, thermal parameters and cytotoxicity of Sn-0.7Cu eutectic solder alloys. Mater Charact. 2023;205:113337. http://doi.org/10.1016/j.matchar.2023.113337.
17. He P, Lu XC, Lin T, Li H, An J, Ma X, et al. Improvement of mechanical properties of Sn–58Bi alloy with multi-walled carbon nanotubes. Trans Nonferrous Met Soc China. 2012;22:s692-6. http://doi.org/10.1016/S1003-6326(12)61788-9.
18. Lin S, Nguyen TL, Wu S, Wang Y. Effective suppression of interfacial intermetallic compound growth between Sn–58 wt.% Bi solders and Cu substrates by minor Ga addition. J Alloys Compd. 2014;586:319-27. http://doi.org/10.1016/j.jallcom.2013.10.035.
19. Chen X, Zhou J, Xue F, Yao Y. Mechanical deformation behavior and mechanism of Sn-58Bi solder alloys under different temperatures and strain rates. Mater Sci Eng A. 2016;662:251-7. http://doi.org/10.1016/j.msea.2016.03.072.
20. Liu Y, Tu KN. Low melting point solders based on Sn, Bi, and In elements. Mater. Today Advances. 2020;8:100115. http://doi.org/10.1016/j.mtadv.2020.100115.
21. Hou Z, Zhao X, Wang Y, Gu Y, Tan C, Xie X, et al. Alloying regulation mechanism toward microstructure evolution of Sn-bi-based solder joint under current stress. Mater Charact. 2022;191:112094. http://doi.org/10.1016/j.matchar.2022.112094.
22. Kang H, Rajendran SH, Jung JP. Low melting temperature Sn-Bi solder: effect of alloying and nanoparticle addition on the microstructural, thermal, interfacial bonding, and mechanical characteristics. Metals. 2021;11(2):364. http://doi.org/10.3390/met11020364.
23. Wang F, Lv Z, Sun L, Chen H, Li M. Microstructure changes in Sn-Bi solder joints reinforced with Zn@Sn particles in thermal cycling and thermomigration. J Taiwan Inst Chem Eng. 2023;146:104871. http://doi.org/10.1016/j.jtice.2023.104871.
24. Hmadeh L, Jaculli MA, Elahifar B, Sangesland S. Development of bismuth-based solutions for well plugging and abandonment: a review. Pet Res. 2024;9(2):250-64. http://doi.org/10.1016/j.ptlrs.2024.01.003.
25. Lee TK, Xie W, Tsai M, Sheikh MD. Impact of microstructure evolution on the long-term reliability of wafer-level chip-scale package Sn–Ag–Cu solder interconnects. IEEE Trans Compon Packaging Manuf Technol. 2020;10(10):1594-603. http://doi.org/10.1109/TCPMT.2020.3016870.
26. Tümer M, Warchomicka FG, Pahr H, Enzinger N. Mechanical and microstructural characterization of solid wire undermatched multilayer welded S1100MC in different positions. J Manuf Process. 2022;73:849-60. http://doi.org/10.1016/j.jmapro.2021.11.021.
27. Zhou Q, Lee TK, Bieler TR. In-situ characterization of solidification and microstructural evolution during interrupted thermal fatigue in SAC305 and SAC105 solder joints using high energy X-ray diffraction and post-mortem EBSD analysis. Mater Sci Eng A. 2021;802:140584. http://doi.org/10.1016/j.msea.2020.140584.
28. Poon NM, Wu CML, Lai JKL, Chan YC. Residual shear strength of Sn-Ag and Sn-Bi leadfree SMT joints after thermal shock. IEEE Trans Adv Packag. 2000;23(4):708-14. http://doi.org/10.1109/6040.883762.
29. Miao HW, Duh J. Microstructure evolution in Sn-Bi and Sn-Bi-Cu solder joints under thermal aging. Mater Chem Phys. 2001;71(3):255-71. http://doi.org/10.1016/S0254-0584(01)00298-X.
30. Wang F, Luktuke A, Chawla N. Microstructural coarsening and mechanical properties of eutectic Sn-58Bi solder joint during aging. J Electron Mater. 2021;50(12):6607-14. http://doi.org/10.1007/s11664-021-09255-2.
31. Raeder CH, Felton LE, Tanzi VA, Knorr DB. The effect of aging on microstructure, room temperature deformation, and fracture of Sn-Bi/Cu solder joints. J Electron Mater. 1994;23(7):611-7. http://doi.org/10.1007/BF02653346.
32. Dantas SLA, Souza ALR, Spinelli JE, Correa MA, Silva BL. Tailoring microstructural and electrical properties of hypoeutectic sn-cu through ni doping. J Electron Mater. 2023;52(12):7972-8. http://doi.org/10.1007/s11664-023-10713-2.
33. Silva BL, Silva VCE, Garcia A, Spinelli JE. Effects of Solidification thermal parameters on microstructure and mechanical properties of Sn-Bi solder alloys. J Electron Mater. 2017;46(3):1754-69. http://doi.org/10.1007/s11664-016-5225-7.

34. Bogno A-A, Spinelli JE, Afonso CRM, Henein H. Microstructural and mechanical properties analysis of extruded Sn–0.7Cu solder alloy. J Mater Res Technol. 2015;4(1):84-92. http://doi.org/10.1016/j.jmrt.2014.12.005.
35. Freitas ES, Osorio WR, Spinelli JE, Garcia A. Mechanical and corrosion resistances of a Sn–0.7 wt.%Cu lead-free solder alloy. Microelectron Reliab. 2014;54(6-7):1392-400. http://doi.org/10.1016/j.microrel.2014.02.014.
36. Xian JW, Belyakov SA, Gourlay CM. Time-lapse imaging of Ag_3Sn thermal coarsening in Sn-3Ag-0.5Cu solder joints. J Electron Mater. 2021;50(3):786-95. http://doi.org/10.1007/s11664-020-08498-9.
37. Morando C, Fornaro O. Influence of aging on microstructure and hardness of lead-free solder alloys. Solder Surf Mt Technol. 2021;33(1):57-64. http://doi.org/10.1108/SSMT-03-2020-0013.
38. Libot JB, Alexis J, Dalverny O, Arnaud L, Milesi P, Dulondel F. Microstructural evolutions of Sn-3.0Ag-0.5Cu solder joints during thermal cycling. Microelectron Reliab. 2018;83:64-76. http://doi.org/10.1016/j.microrel.2018.02.009.
39. Lee DJ, Kang C-S, Baek DH, Lee KK, Moon K-W, Handwerker CA. Effects of aging on interface mechanical properties of solder joints of Sn-3.5Ag and Sn-3.5Ag-1.0Zn solder alloys. J Jpn Inst Met Mater. 2021;85(12):357-65. http://doi.org/10.2320/jinstmet.J2021021.
40. Gain AK, Zhang L. Effect of isothermal aging on microstructure, electrical resistivity and damping properties of Sn–Ag–Cu solder. J Mater Sci Mater Electron. 2017;28(13):9363-70. http://doi.org/10.1007/s10854-017-6675-2.
41. McCartney DG, Hunt JD. Measurements of cells and primary dendrite arm spacing in directionally solidified aluminium alloys. Acta Metall. 1981;29(11):1851-63. http://doi.org/10.1016/0001-6160(81)90111-5.
42. Nishikawa H, Hirata Y, Yang CH, Lin SK. Effect of low Bi content on reliability of sn-bi alloy joints before and after thermal aging. J Miner Met Mater Soc. 2022;74(4):1751-9. http://doi.org/10.1007/s11837-021-05146-3.
43. Hou Z, Zhao X, Wang Y, Gu Y, Tan C, Xie X, et al. Alloying regulation mechanism toward microstructure evolution of Sn-bi-based solder joint under current stress. Mater Charact. 2022;191:112094. http://doi.org/10.1016/j.matchar.2022.112094.
44. Minho O, Tanaka Y, Kobayashi E. Microstructure evolution at the interface between Cu and eutectic SneBi alloy with the addition of Ag or Ni. J Mater Res Technol. 2023;26:8165-80. http://doi.org/10.1016/j.jmrt.2023.09.159.
45. Lee BJ, Oh CS, Shim JH. Thermodynamic assessments of the Sn-In and Sn-Bi binary systems. J Electron Mater. 1996;25(6):983-91. http://doi.org/10.1007/BF02666734.
46. Delhaise AM, Chen Z, Perovic DD. Solid-state diffusion of Bi in Sn: effects of anisotropy, temperature, and high diffusivity pathways. J Miner Met Mater Soc. 2019;71(1):133-42. http://doi.org/10.1007/s11837-018-3145-0.
47. Goldstein JI, Newbury DE, Joy DC, Lyman CE, Echlin P, Lifshin E, et al. Scanning electron microscopy and X-ray microanalysis. New York: Springer; 2017.

Data Availability

The dataset supporting the findings of this study is not publicly available.